

Direct measurement of relative permeability in rocks from unsteady-state saturation profiles



Amir Kianinejad*, Xiongyu Chen, David A. DiCarlo

Department of Petroleum and Geosystems Engineering, The University of Texas at Austin, Austin, Texas, USA

ARTICLE INFO

Article history:

Received 6 October 2015

Revised 25 April 2016

Accepted 26 April 2016

Available online 29 April 2016

Keywords:

Relative permeability

Gravity drainage

Unsteady-state

Consolidated rock

ABSTRACT

We develop a method to measure liquid relative permeability in rocks directly from transient in situ saturation profiles during gravity drainage experiments. Previously, similar methods have been used for sandpicks; here, this method is extended to rocks by applying a slight overpressure of gas at the inlet. Relative permeabilities are obtained in a 60 cm long vertical Berea sandstone core during gravity drainage, directly from the measured unsteady-state in situ saturations along the core at different times. It is shown that for obtaining relative permeability using this method, if certain criteria are met, the capillary pressure of the rock can be neglected. However, it is essential to use a correct gas pressure gradient along the core. This involves incorporating the pressure drop at the outlet of the core due to capillary discontinuity effects. The method developed in this work obtains relative permeabilities in unsteady-state fashion over a wide range of saturations quickly and accurately.

© 2016 Elsevier Ltd. All rights reserved.

1. Introduction

Along with pressure-saturation measurements, relative permeability of a particular media is a crucial multi-phase property. But relative permeability measurements are difficult, time consuming, and expensive endeavors, especially for three-phase flow (Grader and O'Meara Jr, 1988; Honarpour and Mahmood, 1988; Oak et al., 1990). Moreover, the obtained data are sometimes not representative of the exact processes occurring in the reservoirs due to limitations, interpretations, and assumptions attributed to each measurement method (Geffen et al., 1951; Richardson et al., 1952; Jones and Roszelle, 1978; Oak, 1990; Mohanty and Miller, 1991; Fassihi and Potter, 2009).

The steady-state method was the first method proposed for two- and later three-phase relative permeability measurement (Osoba et al., 1951; Geffen et al., 1951; Richardson et al., 1952; Braun and Blackwell, 1981). However, this method is time consuming, expensive, and only provides a limited number of points on the relative permeability curve. In addition, careful attention must be paid to the design of these experiments to minimize the saturation gradients at the outlet side of the core due to capillary end effects (Osoba et al., 1951; Richardson et al., 1952; Rapoport and Leas, 1953).

As an alternative for faster measurements, unsteady-state methods have been proposed and used (Welge, 1950; Johnson et al., 1959; Sarem, 1966; Saraf et al., 1982; Virnovskii, 1984; Grader and O'Meara Jr, 1988; Siddiqui et al., 1996). These methods allow the phase saturations to change naturally. Consequently, these methods can potentially mimic flow processes occurring in reservoirs better than steady-state methods, since steady-state methods pre-determine the flow rates of fluids. However, the calculation of relative permeability from unsteady-state experiments require assumptions and interpretations of the measured pressure drops and effluent fractional flows, which may not necessarily hold (Mohanty and Miller, 1991). Particularly, the measured fractional flows in the effluent may be altered by capillary end effects, thus the pressure gradient measured across the core may be very different than the local pressure gradients of each phase (Geffen et al., 1951; Osoba et al., 1951; Richardson et al., 1952; Rapoport and Leas, 1953).

It is also possible to calculate relative permeabilities by history matching data; these data can be pressure, production, or saturation data measured during unsteady-state flooding experiments (Maini and Batycky, 1985; Maini and Okazawa, 1987; Vizika and Lombard, 1996). However, the calculated relative permeabilities are susceptible to errors due to local heterogeneity and capillarity. In addition, the resulting relative permeability curves are not unique, which is characteristic of inverse methods (Sigmund and McCaffery, 1979; Kerig and Watson, 1987).

Recently, Sahni et al. (1998) and others (Naylor et al., 1996; DiCarlo et al., 2000a; DiCarlo et al., 2000b; Dehghanpour et al., 2011; Dehghanpour and DiCarlo, 2013a; Kianinejad et al., 2014)

* Corresponding author.

E-mail address: kianinejad.amir@utexas.edu (A. Kianinejad).

Nomenclature

g	gravity, m/s^2
k	absolute permeability, m^2
k_{ri}	relative permeability to phase i , dimensionless
P_c	capillary pressure, Pa
$P_{c_{entry}}$	entry capillary pressure, Pa
P_i	pressure of phase i , Pa
S_i	saturation of phase i , dimensionless
S_{wr}	residual water saturation, dimensionless
u_i	flux of phase i , m/s
z	position along the core, m
t	time, s

Greek letters

λ	Brooks–Corey exponent, dimensionless
μ_i	viscosity of phase i , cp
ρ_i	density of phase i , kg/m^3
Φ_i	potential of phase i , Pa
ϕ	porosity, dimensionless

Subscripts

i	phase
g	gas
w	water

obtained relative permeabilities from saturation profiles during gravity drainage experiments in vertical sandpacks. They showed that if particular criteria are met, the capillary pressure gradients can be neglected and relative permeabilities can be obtained directly from in situ saturation profiles. Using this method, they obtained many relative permeability data points over a range of saturations; this is opposed to other methods which only provide a limited number of points over the saturation space. However, this method suffered from the following issues:

- It was only applicable to unconsolidated sandpacks with low capillary forces.
- The saturation path of the experiments in three-phase space was chosen by nature, and they did not have any control on the saturation path of their experiments.
- It only obtained relative permeabilities at low saturations ($S < 0.3$), due to fast saturation changes at early times of the experiments.

In reservoirs, there is no practical difference between consolidated rocks and unconsolidated sands as the fluid column height is large enough to create high driving forces solely due to gravity (Hagoort, 1980; Naylor et al., 1996; Zhou and Blunt, 1997; Rezaei et al., 2010; Mohsenzadeh et al., 2011). But in the laboratory, rocks require long cores (>1 m) so that the fluid column pressure can exceed the entry capillary pressure of the core, and the fluids inside the core can flow by gravity. It is practically impossible to have long cores in laboratory, and shorter cores show no fluid movement due to insufficient fluid column pressures. This is why only sandpacks have been used in laboratory experiments (Sahni et al., 1998; DiCarlo et al., 2000a; Dehghanpour et al., 2010; Dehghanpour et al., 2011; Kianinejad et al., 2014). Sandpacks have smaller capillary forces, thus fluids can drain by gravity even in shorter columns.

In this work, we extend this gravity drainage method to consolidated rocks by using a small gas pressure gradient to overcome the capillary entry pressure. With this extension, we obtain relative permeabilities in consolidated rocks in unsteady-state gravity driven experiments, directly from the measured in situ saturations along the core samples. We measure two-phase water relative permeability in a 60 cm long Berea sandstone core. Although we inject

gas from the top, the drainage process is still a gravity-dominated process; the injected gas is only to allow the in situ fluids (water/oil) to drain by gravity.

2. Theory and formulation

The gravity drainage method for obtaining relative permeability has been shown to work well in sandpacks (Sahni et al., 1998; DiCarlo et al., 2000a; DiCarlo et al., 2000b; Dehghanpour and DiCarlo, 2013b; Kianinejad et al., 2015). The basic idea is to fill the column with liquid; open up the bottom and top to let liquid flow out and gas to flow in; and measure the saturation of the liquid phase i as a function of space and time, $S_i(z, t)$. Using these data, the flux of phase i is found using mass conservation. The relative permeability as a function of saturation is then calculated directly from the definition of relative permeability

$$k_{ri} = -u_i \left(\frac{k}{\mu_i} \frac{d\Phi_i}{dz} \right)^{-1} \quad (1)$$

where u ($[LT^{-1}]$) is fluid flux, k is permeability ($[L^2]$), k_r ($[-]$) is relative permeability, μ ($[ML^{-1}T^{-1}]$) is viscosity, Φ is fluid potential ($[ML^{-1}T^{-2}]$), and z ($[L]$) is position along the core. Subscript i denotes phase.

Needed in this calculation is the potential gradient. For sandpacks draining under gravity, it has been shown that for the center section of a 1 m long column, this gradient can be estimated to be the gravitational gradient, $\rho_i g$ (Sahni et al., 1998; DiCarlo et al., 2000a; Dehghanpour and DiCarlo, 2013a; Kianinejad et al., 2014). This is the case when one liquid phase (oil or water) drains (being replaced by gas), and also when two liquid phases (oil and water) drain.

Conceptually, this method also works for consolidated rocks. Measuring the saturation as a function of space and time (and calculating the fluxes) is exactly the same for rocks as it is for sandpacks. The difficulty for rocks arises in determining the potential gradient.

In practice, this method fails for the simple reason that if the core is 60 cm of length – which in practice is a long laboratory core – capillary forces hold in the liquid and do not allow gas to penetrate the core. Mathematically, it is equivalent to say that for rocks, the gas entry pressure is greater than the maximum gravitational potential. Or in terms of Eq. (1), the gradient of the total potential ($\Phi_i = P_i + \rho_i g z$) is zero throughout the column, and thus there is no flow. Clearly, if the core remains saturated with liquid, this precludes a relative permeability measurement. If the core was longer, this issue would greatly lessen, but cores longer than 60 cm are hard to handle and must be obtained from outcrops.

Thus the goal in any drainage relative permeability measurement in rocks is to make sure that one can: (a) get gas into the core and allow flow of the liquid(s), and (b) estimate the gradient of the liquid phases accurately.

We accomplish this by injecting gas at the inlet at a pressure greater than the outlet gas pressure. This excess gas pressure is chosen to overcome the gas entry pressure, thus allowing the column to drain. In the following, we show how we can calculate the liquid pressure gradient under this combined gas injection and gravity drainage scenario.

Substituting the definition of capillary pressure ($P_c = P_g - P_l$) into the total modified pressure, and taking the gradient gives

$$\frac{d\Phi_i}{dz}(z, t) = \frac{dP_g(z, t)}{dz} + \rho_i g - \frac{dP_c(z, t)}{dz} \quad (2)$$

where P_g ($[ML^{-1}T^{-2}]$) is the gas pressure, ρ_i ($[ML^{-3}]$) is the liquid phase density (which is assumed to be much greater than the gas phase density), and P_c ($[ML^{-1}T^{-2}]$) is the capillary pressure, which is dependent on the saturation of phase i .

In estimating the contributions to the total gradient on the right hand side, we first note that the gravity gradient ($\rho_i g$) is constant and known throughout the column. This is the main driving force in sandpack gravity drainage experiments. Here, the capillary pressure gradient ($\frac{dP_c}{dz}$) and the gas pressure gradient ($\frac{dP_g}{dz}$) terms need to be expressed in comparison to the gravity gradient.

First, consider the capillary pressure gradient. If the pressure-saturation curve is known, this can be estimated from the observed saturation profiles using the chain rule

$$\frac{dP_c(z, t)}{dz} = \frac{dP_c}{dS} \frac{\partial S(z, t)}{\partial z} \quad (3)$$

Although ostensibly straightforward, the difficulty lies in taking spatial derivatives of the saturation data, as when data exhibit any sort of fluctuations or “noise” caused by heterogeneities, their derivatives amplify the noise. Instead of directly calculating this gradient, we look for regions in the profile where on a global scale $\frac{dP_c(z, t)}{dz} \ll \rho g$, or equivalently $\frac{\partial S(z, t)}{\partial z} \ll \rho g \left(\frac{dP_c}{dS}\right)^{-1}$. In this case, the capillary pressure gradient is small enough to be ignored. In sandpacks, it has been shown (Kianinejad et al., 2015) that this saturation gradient condition is met in regions of the column:

- Away from (>15 cm) entry and exit of the core;
- Behind (>15 cm) the moving drainage front.

Simply, in these regions, the saturation profiles in sandpacks are relatively “flat” with space. Independent pressure measurements have confirmed that in these regions the capillary pressure gradient is much lower than the gravitational gradient (DiCarlo, 2003). Thus in this work, we attempt to see if we can get “flat” saturation regions in rocks by injecting gas. As will be shown, we find that above a certain injection pressure, this condition can be met in rocks.

Next, consider the gas pressure gradient, $\frac{dP_g}{dz}$. In previous relative permeability measurements in sandpacks using this method, gas was not forced in, and the pressure gradient for the gas phase was assumed to be negligible compared to the gravitational gradient, because $\mu_g \ll \mu_l$ (Sahni et al., 1998; DiCarlo et al., 2000b; Dehghanpour et al., 2011; Kianinejad et al., 2014). This is a common assumption for flow in soils or sandpacks, as is shown in Richards’ equation (Richards, 1931) for water movement in unconsolidated soils. However, in this work, by injecting gas at pressures higher than entry pressure, we create non-negligible gas pressure gradients. Fortunately, this gradient is relatively uniform in the bulk of the core, and can be estimated from measurements and straightforward multi-phase modeling. Still, it is advantageous to use lower injection pressures, as we still want the gravitational gradient to dominate, and the higher the injection pressure the higher the gradient. Later in this text, we show how this term is estimated and included in the calculations.

As mentioned above, calculating the flux from the saturation profile and the other parameters needed to obtain the relative permeability are straightforward. From mass conservation, the fluid flux ($u_i(z, t)$) as a function of space and time is found from the saturation profiles as follows (Kianinejad et al., 2015):

$$u_i(z^*, t_{j+1/2}) = \frac{\int_{z=0}^{z^*} ([S_i(z, t_{j+1}) - S_i(z, t_j)] \phi dz)}{t_{j+1} - t_j} \quad (4)$$

where S ([–]) is fluid saturation, ϕ ([–]) is porosity, and t ([T]) is time. Subscript j denotes time step.

The rest of the parameters in Eq. (1), i.e. the core’s absolute permeability, and fluid density and viscosity, can be easily measured outside of the drainage experiment. Once all the required parameters are obtained from the measured saturation profiles, relative permeabilities at discrete points can be calculated through Eq. (1) at the sections of the core which meet the above mentioned criteria. In particular, the relative permeability data mea-

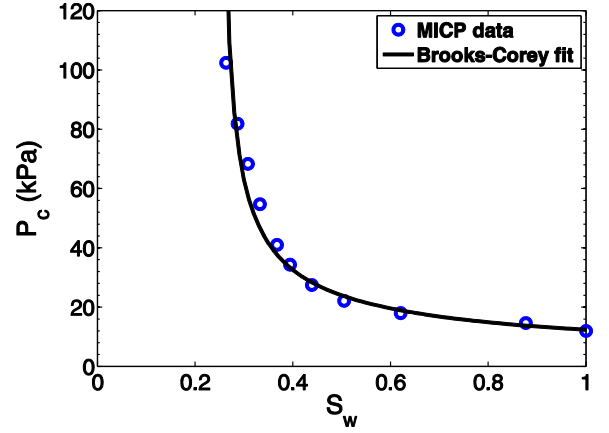


Fig. 1. Capillary pressure-saturation curve of the Berea core: experimental data obtained through the mercury intrusion capillary pressure method (MICP) and the Brooks–Corey model best fit.

sured in this work are obtained from the saturation data at the middle 20 cm ($z = 20 - 40$ cm) of our 60 cm long Berea core where the mentioned criteria are met.

It should be noted that the same principles can be applied to three-phase systems to measure relative permeability of two liquid phases, e.g. water and oil. However, the relative permeability of the gaseous phase cannot be obtained, as the flux of the gas phase is not measured during the experiments (gas is being injected at constant pressure). In addition, this method is not applicable to liquid-liquid systems, e.g. two-phase oil/water system; the criteria mentioned above will not be met as the differences in density and viscosity of the two liquid phases is much smaller; one of the key factors in this method is that the injected phase should have a relatively low viscosity. Moreover, this method requires long cores for two reasons: (a) to provide enough room for saturations to develop spatially uniform (flat) sections, and (b) to have these sections away from the capillary discontinuity at the inlet and outlet of the core.

3. Materials

3.1. Rock sample

A single Berea sandstone core was used for all the experiments presented in this work. The Berea core was 60 cm long and 7.6 cm in diameter, with a uniform porosity of 0.215 along the core measured by CT scanning. The permeability of the Berea sandstone sample used in the experiments was measured as 300 mD from a separate core sample cut from the same Berea block with 24.1 cm length and 3.8 cm diameter. Capillary pressure of the rock sample was measured using the mercury intrusion capillary pressure (MICP) method. Fig. 1 shows the measured capillary pressure curve and the Brooks–Corey fit to the experimental data after converting the raw data to the water-gas system using corrections explained by Pini and Benson (2013). The Brooks–Corey model (Brooks and Corey, 1964)

$$P_{c_{gw}} = P_{c_{entry}} \left(\frac{1 - S_{wr}}{S_w - S_{wr}} \right)^{1/\lambda} \quad (5)$$

fits the experimental data with $P_{c_{entry}} = 13.8$ kPa (2 psi), $S_{wr} = 0.25$, and $\lambda = 1.66$.

3.2. Fluids

A light brine (1 wt% sodium bromide aqueous solution) was used for all two-phase water/gas experiments as the aqueous

Table 1
Physical properties of the fluids used in the experiments.

Fluid	Density (kg/m ³)	Viscosity (cp)
Light brine (1 wt% NaBr)	1006	1.02
Air	1.2	0.02

Table 2
Two-phase experiments with different initial and conducting conditions.

Test	Type of drainage	Gas injection pressure (kPa)
1	Primary	8.27
2	Secondary	26.06
3	Secondary	42.26
4	Secondary	61.77
5	Primary	61.77

phase, while air was used as the gas phase. The physical properties of the fluids are summarized in Table 1.

4. Methods

4.1. Fluid calibrations

To calculate fluid saturations during the experiments, calibrations at one x-ray energy (100 kV) were required. The calibrations for gas and brine saturated core were obtained once the core was completely dry (100% gas saturated), and once when the core was completely saturated with brine.

4.2. Saturation measurement

Using a vertical positioning system, the core was moved vertically and scanned at different positions with 2 cm intervals from top to the bottom. Since the experiments involved two phases, the core was scanned at only one energy level to measure the in situ saturations along the core during the experiments. Combining the measured CT values with the fact that summation of water and gas saturations equals to one, fluid saturations along the core were calculated at different times, $S_i(z, t)$ (Krevor et al., 2012).

4.3. Experimental procedure

In this work, five two-phase, water/gas gravity drainage experiments were conducted on a single Berea core sample. Each experiment was conducted under a different injection pressure to investigate the effect of injection pressure on saturation profiles, and obtained relative permeabilities, with Test 1 being at the lowest pressure and Test 5 at the highest. To prepare the core for Test 1, the core was vacuumed from the top for several hours, and then was completely saturated with brine injecting from the bottom. In Test 1 gas was injected from the top of the core at 8.27 kPa (1.2 psig). Tests 2–4 started from the initial condition of residual gas: these tests had gas injected at pressures of 26.06, 42.26, and 61.77 kPa (3.78, 6.13, and 8.96 psig), respectively. For Test 5, the core was restored to 100% brine saturation the same way as that of Test 1; then gas was injected at 61.77 kPa (8.96 psig). The initial and operating conditions of the experiments are listed in Table 2.

During all the experiments, the core was vertically oriented with the outlet of the core open to the atmosphere. The injected gas was first bubbled through a column of water before entering the core to equilibrate the gas with water vapor and avoid any saturation changes due to evaporation of fluids inside the core.

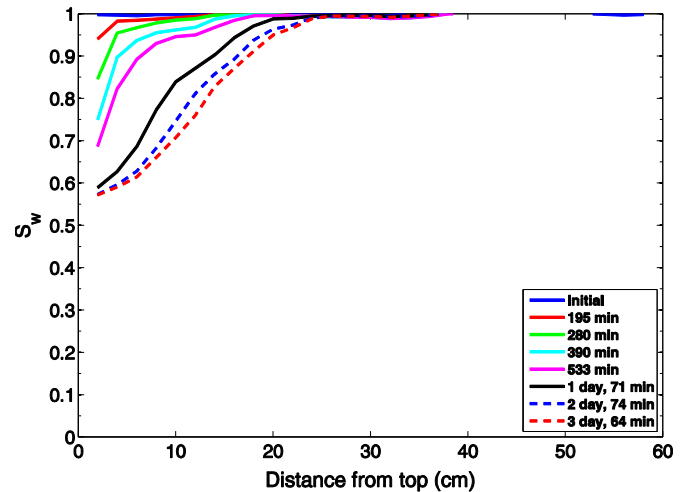


Fig. 2. Water saturation profile along the core at different times during two-phase water/gas experiment Test 1.

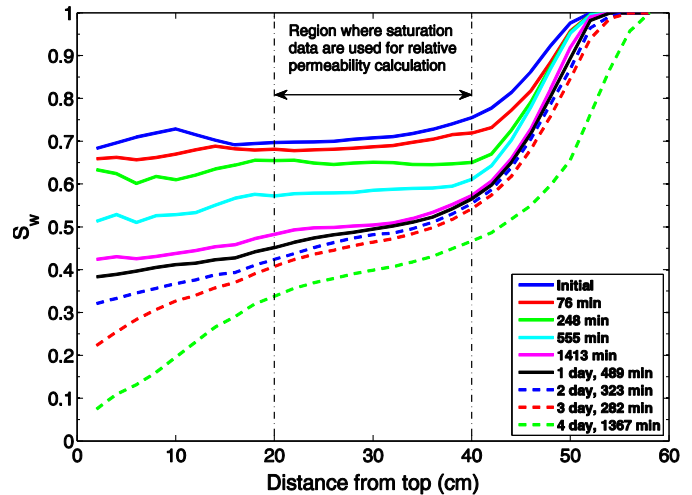


Fig. 3. Water saturation profile along the core at different times during two-phase water/gas experiment Test 2. The dash-dotted lines show the region of the core from which the saturation data are used to calculate relative permeability.

5. Results

5.1. Saturation vs. space and time

We first show how the saturation profiles develop in time for each drainage as a function of applied gas pressure. Fig. 2 shows the water saturation profile along the core during the primary drainage ($S_{wi} = 1$) experiment (Test 1) with the lowest gas injection pressure (1.2 psig or 8.27 kPa). Here, the gas enters the core, but the gas front stops at $z=25$ cm; below this height water is still being held by capillary forces.

In the next four experiments, each drainage used a higher gas injection pressure. The goal was to move the drainage front further down, and see how the injection pressure affects the saturation profiles in (a) providing more spatial room for saturations to change along the core, and (b) obtaining spatially uniform saturation regions which meet the capillary criteria for calculating relative permeabilities.

Figs. 3–6 show the water saturation profiles in time for these experiments with sequentially increasing gas injection pressures. Fig. 3 shows Test 2 which was conducted at a slightly higher injection pressure (3.78 psig or 26.06 kPa). Comparing Fig. 3 with

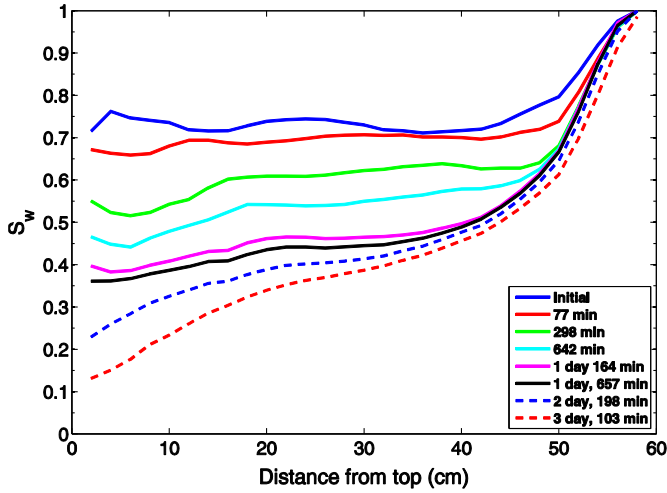


Fig. 4. Water saturation profile along the core at different times during two-phase water/gas experiment Test 3.

Fig. 2 shows that injecting gas at 26.06 kPa drives the water front all the way down to the bottom of the core, while the capillary end effect reduces to the bottom 20 cm of the core.

Figs. 4–6 show Tests 3–5 at gas injection pressures of 42.26, 61.77, and 61.77 kPa respectively. In these figures, with increasing pressure, the capillary end effect is moved further down the column. This also yields a longer region in the column where the saturation is relatively constant in space.

Clearly, the profiles are slightly different with different injection pressures; the question now becomes accurately obtaining relative permeability from these profiles. As mentioned in Section 2, this comes down to obtaining the overall modified pressure gradient; i.e. the sizes of the capillary pressure gradient and the gas pressure gradient. We first look at the gas pressure gradient.

5.2. Gas pressure gradient

As mentioned above earlier, the previous studies that used gravity drainage method to measure relative permeabilities in unconsolidated sandpacks (Sahni et al., 1998; DiCarlo et al., 2000a; DiCarlo et al., 2000b; Dehghanpour and DiCarlo, 2013b; Dehghanpour and DiCarlo, 2013a; Kianinejad et al., 2014) neglected the gas pressure gradient term, $\frac{dp_g(z,t)}{dz}$, since the pressure gradient of the gas phase was considerably smaller than the gravitational gradient, $\rho_i g$ (Kianinejad et al., 2015).

In contrast, the injection gas pressures in this study are significant compared to the gravitational gradient, and cannot be neglected. In this work, $\rho_w g = 9.86 \frac{\text{kPa}}{\text{m}}$ while injection gas pressures in our 60 cm long core of Berea sandstone during Tests 2–5 are 26.06, 42.26, 61.77, and 61.77 kPa, respectively. This yields to overall gas pressure drops per length of 43.4, 70.4, 103, and 103 $\frac{\text{kPa}}{\text{m}}$, respectively.

However, it is necessary to evaluate the local gas pressure gradient, $\frac{dp_g(z,t)}{dz}$, for each experiment at the middle section of the core. It is well known that due to capillary discontinuity at the outlet of the core, there will be wetting phase hold up and large saturation gradients at the outlet, regardless of the measurement method (Osoba et al., 1951; Richardson et al., 1952; Rapoport and Leas, 1953). This behavior is seen in many studies including the current study, shown in Figs. 3–6. Due to this capillary hold up at the outlet, a large part of the pressure drop during core floods occurs in the last few centimeters of the core.

The same end effect is observed in this study. As shown in Figs. 3–6, there exists a water hold-up region in the bottom 10–

20 cm of the core due to capillary end effect (capillary discontinuity). To estimate the pressure drop in this end region and use the correct value of pressure gradient in the middle 20 cm of the core, we ran numerical simulations using our in-house simulator to obtain the correct gas pressure gradient in the middle section of our core. Fig. 7 shows the gas pressure along the core at different times for gas injection pressures of 26.06, 42.26, and 61.77 kPa, the same values as those used in Tests 2–5, respectively. Fig. 7 shows that, after the passage of the gas front to the bottom, the gas pressure gradient at each position along the core did not change with time during the entire experiment. It is evident in Fig. 7 that there is a sharp pressure drop at the bottom of the core, which is due to capillary end effect mentioned above. To obtain the water relative permeabilities for Tests 2–5 (discussed in the following), we first found the gas pressure gradient associated with the middle 20 cm of the core ($z=20\text{--}40\text{ cm}$) for each experiment. The dashed lines in Fig. 7 show the slope of the gas pressure profile for each experiment at the middle of the core. The local gas pressure gradients shown in Fig. 7 are $\frac{dp_g}{dz} = 14.7, 35.5, \text{ and } 61.6 \frac{\text{kPa}}{\text{m}}$, corresponding to those used in Tests 2–4, respectively. The gas pressure gradient of Test 5 is the same as that of Test 4. These values are significantly smaller than the overall pressure gradients mentioned earlier; simply, a large portion of the overall pressure drop is taken up in the end effect.

To determine gas pressure gradient in the middle of the core, we used a wide range of water and gas relative permeability curves to examine the sensitivity of the gas pressure gradient on the input relative permeabilities. We used gas relative permeabilities ranging from $k_{rg} = 0.1 \times S_g^2$ to $k_{rg} = S_g^2$, and $k_{rg} = 0.1 \times S_g^3$ to $k_{rg} = S_g^3$; and water relative permeabilities from $k_{rw} = 0.1 \times S_w^3$ to $k_{rw} = S_w^6$. Our results show that, the gas pressure gradient changes less than 0.35%, 1.53%, and 2.5% for Tests 2–4, respectively, for the given range of relative permeabilities. These changes in pressure gradients translate into less than 0.25%, 1.2%, and 2.1% change in calculated relative permeabilities, respectively. These small changes confirm the robustness of the estimated gas pressure gradients for relative permeability calculations.

5.3. Capillary pressure gradient

For the capillary pressure gradient, the ideal case is to find regions of the column where it is much less than the gravitational gradient. This is equivalent to finding regions where the saturation is “flat” or more exactly the spatial saturation gradient is small, since a small $\frac{dS_w}{dz}$ will lead to a small $\frac{dp_c}{dz}$ through $\frac{dp_c}{dz} = \frac{dp_c}{dS_w} \frac{dS_w}{dz}$. We have P_c vs S_w for the Berea sandstone used (Fig. 1). From this, $|\frac{dp_c}{dS_w}|$ varies between 11 and 146.2 kPa (1.6 and 21.2 psi) depending on the saturation.

Let us look at this criteria in terms of the data shown in Figs. 2–6. For the lowest gas injection pressure (Fig. 2), we see that much of the column was not invaded. For the part that was invaded, we find saturation gradients of $\frac{dS_w}{dz} \geq 0.82\text{m}^{-1}$. For these saturation, $|\frac{dp_c}{dS_w}| \geq 11.7\text{kPa}$ is obtained from the capillary pressure curve of the Berea sandstone sample (Fig. 1). Consequently, the capillary pressure gradient ($|\frac{dp_c}{dz}| = |\frac{dp_c}{dS_w}| \times \frac{dS_w}{dz} \approx 9.6 \frac{\text{kPa}}{\text{m}}$) is comparable to gravitational gradient ($\rho_w g = 9.86 \frac{\text{kPa}}{\text{m}}$), i.e. $\frac{dp_c/dz}{\rho_w g} \approx 1$; these capillary gradients are too large to be ignored. In essence, here the capillary gradient matches the gravitational gradient which stops the flow of water.

The saturation profiles shown in Fig. 3 have a much smaller saturation gradient in the top 40 cm of the core compare to that of Test 1 shown in Fig. 2. As mentioned before, the top 15 cm of the core is affected by the capillary entry effect; in addition, the bottom 20 cm is affected by the capillary end effect. Importantly, the middle 25 cm section of the core meets the criteria mentioned

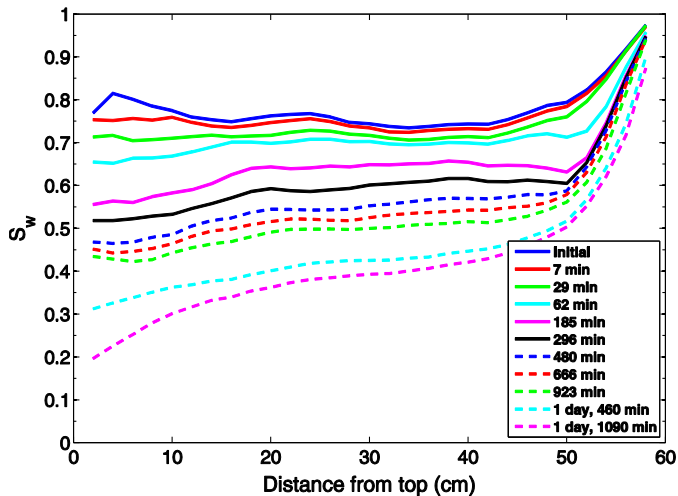


Fig. 5. Water saturation profile along the core at different times during two-phase water/gas experiment Test 4.

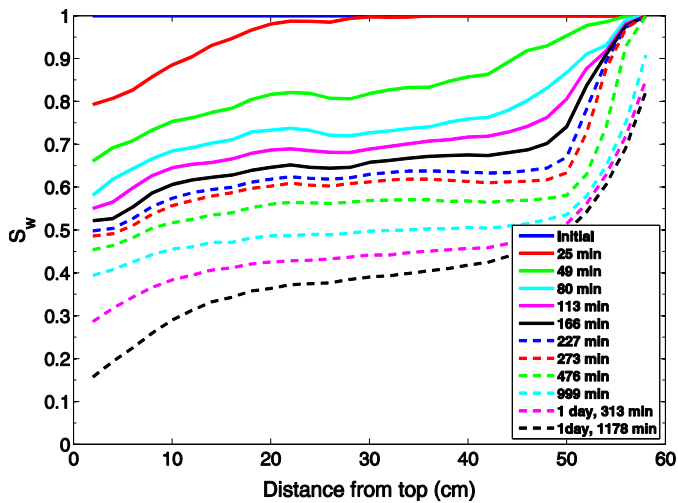


Fig. 6. Water saturation profile along the core at different times during two-phase water/gas experiment Test 5.

above for relative permeability calculations. In this section, the saturation profiles are spatially uniform and have small gradients that result in a negligible capillary pressure gradient. For example, the saturation profile corresponding to $t=76$ min (solid red curve) shown in Fig. 3 has a saturation gradient of $|\frac{dS_w}{dz}| \leq 0.12\text{m}^{-1}$ in the middle 25 cm of the core, far from the entrance and exit of the core. In this section, $\frac{dP_c}{dS_w} \approx -23.03$ kPa, calculated from the measured capillary pressure curve for the rock sample (see Fig. 1). Consequently, $|\frac{dP_c}{dz}| \leq 2.7$ $\frac{\text{kPa}}{\text{m}}$. This is significantly smaller than the gravitation gradient ($\rho_w g = 9.86$ $\frac{\text{kPa}}{\text{m}}$), with $\frac{dP_c/dz}{\rho_w g} \leq 0.28$.

Figs. 4, 5, and 6 show profiles for increasing gas injection pressures of 42.26, 61.77, and 61.77 kPa respectively. In these figures, with increasing pressure, the capillary end effect is moved further down the column, yielding a longer region with a low saturation gradient. As above, these measured saturation gradients can be combined with the capillary pressure curve to obtain estimates of the capillary pressure gradient. For example, for Fig. 4, the saturation gradient corresponding to $t=296$ min is $|\frac{dS_w}{dz}| \leq 0.12\text{m}^{-1}$, yielding a capillary pressure gradient of $|\frac{dP_c}{dz}| \leq 3.8$ $\frac{\text{kPa}}{\text{m}}$ ($\frac{dP_c/dz}{\rho_w g} \leq 0.38$). For Figs. 5 and 6 the values of saturation gradient are even smaller, and yield smaller capillary pressure gradients.

The relative magnitude of the capillary pressure gradient becomes even smaller once the gas pressure gradient is incorporated. In the previous section, the gas pressure gradient is estimated in the middle of the core for each experiment from numerical simulations; as a reminder, in Test 2, the gas pressure gradient in the middle of the core is $\frac{dP_g}{dz} = 14.7$ $\frac{\text{kPa}}{\text{m}}$. Adding the gas pressure gradient to the gravitational gradient, results in the relative magnitude of the capillary pressure gradient of $\frac{dP_c/dz}{dP_g/dz + \rho_w g} \leq 0.11$. This confirms that the capillary pressure gradient for this section is small compared to gas pressure gradient and gravitational gradient, and ignoring capillary gradients in the relative permeabilities results in a bias of 11% or less. Incorporating gas pressure gradient for Test 3–5 shows that if the data are chosen in the low saturation gradient region, the capillary pressure gradient can be ignored with a bias of less than 5%. Table 3 summarizes some examples of saturation and capillary pressure gradients of Test 1–4.

5.4. Water relative permeability

We use the saturation data of the middle 20 cm section of the core to calculate the relative permeabilities of water during the two-phase experiments, Tests 2–5, shown in Figs. 3–6. To obtain relative permeability from each experiment, we used gas pressure gradients of 14.7, 35.5, 61.6, and 61.6 $\frac{\text{kPa}}{\text{m}}$ for Tests 2–5, respectively, corresponding to the value estimated for the middle section of the core in each experiment based on simulation results discussed above. In addition, we considered the gravitational gradient in all the calculations as $\rho_w g = 9.86$ $\frac{\text{kPa}}{\text{m}}$, while neglected the capillary pressure gradient term, ($\frac{dP_c}{dz}$), since it was negligible compared to the gas pressure and gravitational gradients, as discussed above.

In the following, we first show the relative permeabilities obtained from Test 3, and move on to Tests 4 and 5. We then go back to Test 2, because the results of Test 2 are slightly different from those of the other experiments.

Fig. 8 shows the obtained water relative permeability for Test 3, where the gas is being injected at 42.26 kPa. In this figure, the shown relative permeability data correspond to the middle 20 cm section of the core ($z=20$ – 40 cm), for 7 different time intervals; this leads to 60 total data points. From this test, relative permeability is obtained for saturations between 0.3 and 0.7, with the relative permeabilities being between 10^{-3} and 10^{-1} . The overall data follow a normal relative permeability curve obtained from Berea sandstone (comparisons will be shown later).

In Fig. 8 the overall curve is continuous, but there is some minor structure due to the nature of the method. In particular, the data from each time interval (shown in a different color) form a “Γ” shape structure. This structure is discussed in detail later.

Figs. 9 and 10 show the water relative permeabilities obtained from Tests 4 and 5. Again, the data show that at intermediate and high saturations, the data from each time interval line up smoothly together to form a single relative permeability curve. However, for the later time interval measurements, which correspond to lower saturations (see Figs. 5 and 6), the structure of the relative permeability data shifts from following the overall curve to vertical lines. These are essentially the vertical part of the “Γ”.

Fig. 11 shows the relative permeability data obtained for Test 2 which is the lowest injection pressure (26.06 kPa). Here the curve, while in the same overall position, is much more disjointed than the curves at higher pressures. Looking closer at the structure for individual time intervals, the “Γ” shape is still observed, with some intervals showing the vertical leg of the “Γ” shape, and the later times showing the horizontal top.

Fig. 12 shows all the relative permeabilities shown in Figs. 8–11 in a single plot. In this figure, the relative permeabilities from each test show consistent behavior, with the

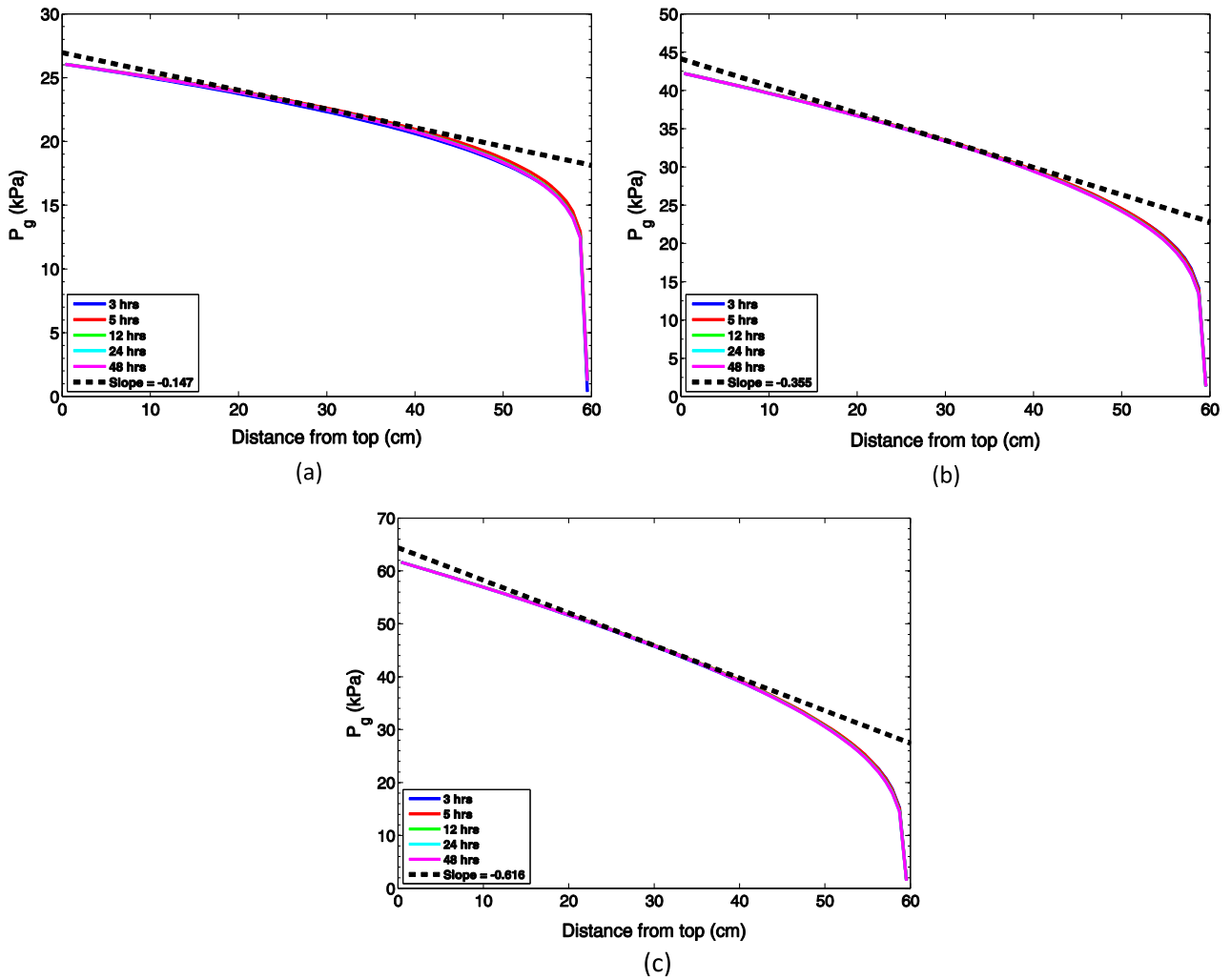


Fig. 7. Gas pressure (gauge pressure) profile along the core at different times for gas injection pressures of (a) 26.06, (b) 42.26, and (c) 61.77 kPa as those of Tests 2–4, respectively. It is also shown in dashed line the slope of the gas pressure profile in the middle of the core.

Table 3
Capillary and gas pressure gradients during each experiment.

Test	Corresponding time of saturation profile (min)	$ \frac{ds_w}{dz} $ (m^{-1})	$ \frac{dP_c}{ds_w} $ (kPa)	$ \frac{dP_g}{dz} $ (kPa/m)	$\frac{dP_c/dz}{\rho_w g}$	$\frac{dP_g/dz}{\rho_w g + dP_c/dz}$
1	Overall	≥ 0.82	≥ 11.7	9.6	≈ 1	≈ 1
2	76	≤ 0.12	≈ 23.03	≤ 2.7	≤ 0.28	≤ 0.11
3	298	≤ 0.12	≈ 30.7	≤ 3.8	≤ 0.38	≤ 0.08
4	62	≤ 0.02	≈ 22.55	≤ 0.45	≤ 0.04	≤ 0.006

measurements done at the highest gas pressure (Test 5) providing data for the highest saturations. Although slight differences among the tests can be observed, (most notably at low saturations), the overall structure is a single relative permeability curve. This shows the robustness of the method; as long as there is enough gas pressure to force the water down the core, the relative permeability will be accurate – there is no need to optimize for a particular pressure.

6. Discussion

In this section, we (a) show how that adding the gas pressure gradient to the relative permeability calculations is necessary, (b) discuss possible reasons for the structure that is seen in the individual relative permeability curves, and (c) compare the data to published data.

6.1. Gas pressure gradient

Earlier in the paper, it is mentioned that previous studies obtained relative permeabilities in sandpacks through gravity drainage experiments by ignoring the gas pressure gradient due to its negligible values compared to gravitational gradient (Sahni et al., 1998; DiCarlo et al., 2000a; DiCarlo et al., 2000b; Dehghanpour and DiCarlo, 2013b; Kianinejad et al., 2014). To show that the gas pressure gradient term must be included in the relative permeability calculations for consolidated rocks, the water relative permeability for Tests 2–5 were calculated also based on considering only fluid gravity while neglecting capillary pressure and gas pressure gradients. Fig. 13 shows relative permeabilities assuming only gravitational gradient. In this figure, two features are evident. First, the relative permeability curve is shifted higher than Fig. 12; some of the data have relative permeabilities over one. Second, the

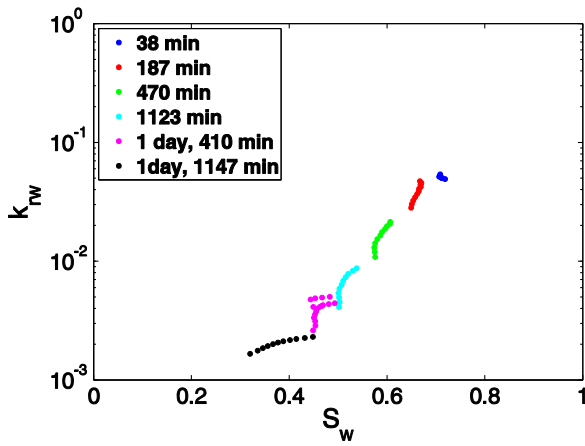


Fig. 8. Water relative permeability during two-phase water/gas experiment Test 3. The times shown in the legend correspond to the middle-time of each of two consecutive saturation profiles shown in Fig. 4.

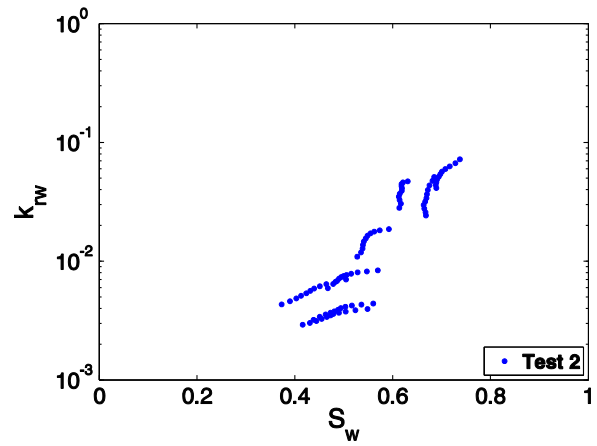


Fig. 11. Water relative permeability during two-phase water/gas experiment Test 2.

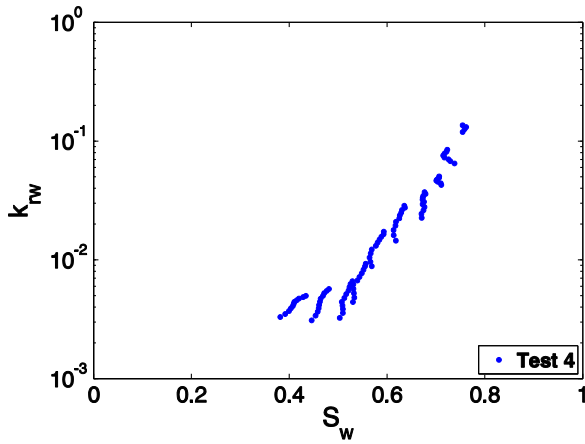


Fig. 9. Water relative permeability during two-phase water/gas experiment Test 4.

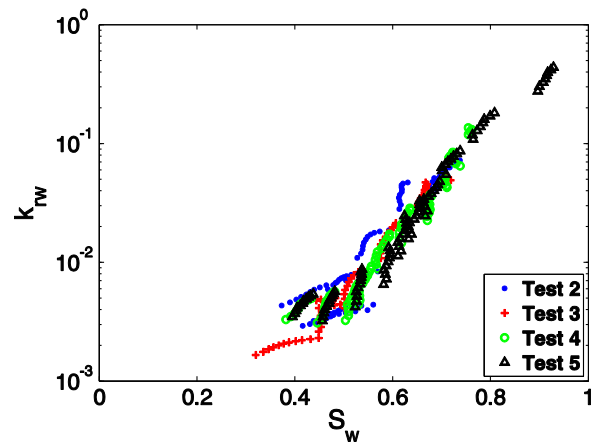


Fig. 12. Water relative permeability obtained from all two-phase experiments, Test 2–5, on log scale.

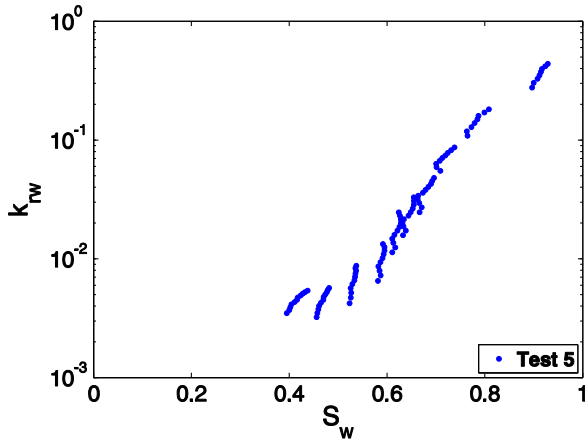


Fig. 10. Water relative permeability during two-phase water/gas experiment Test 5.

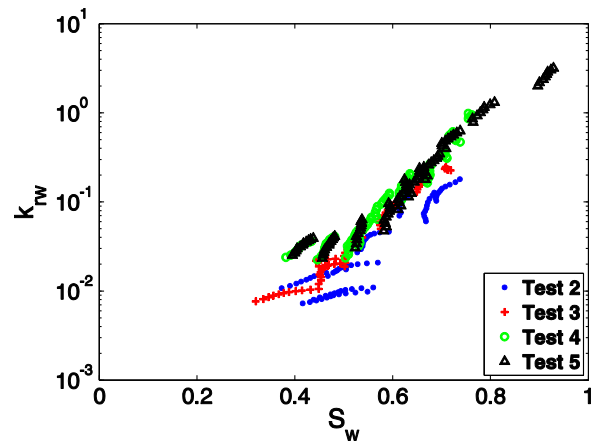


Fig. 13. Water relative permeability calculated by ignoring gas pressure gradients. This is incorrect and yields more scatter and relative permeability values greater than 1.

curves from each test overlap less than they did in Fig. 12. This is simply a fact of having the wrong overall gradient by ignoring the gas pressure gradient. The relative permeabilities above unity result from underestimating the gradient by a factor of 2.5, 4.6, and 7.2 for Tests 2–4, respectively. Since the different tests have different gas gradients, failure to incorporate these gradients results in different curves for different tests in Fig. 13.

6.2. Nature of the structure in relative permeability curves

As pointed out in the results, for each time interval, the set of data points that is obtained tends to show a “Γ” shape. This shape is most likely due to the ignoring of capillary forces, and actually can give us an estimate of when ignoring capillary forces is a reasonable assumption. Taking a step back, essentially each relative permeability point is the measured flux divided by the pressure

gradient, multiplied by some constant normalizing factors (viscosity and permeability). In this method, the flux is obtained from integrating the saturation changes, and the pressure gradient is assumed to be just the gravitational gradient and gas pressure gradient which are constant in time and space. In actuality, the pressure gradient is not constant in time and space, as the capillary gradient does change. If the criteria are met (only data from center 20 cm), the capillary pressure gradient is a small fraction of the overall gradient. But changes in this gradient then may be enough to create the structure of the data that is observed.

In terms of the capillary gradient, it is straightforward to get a rough estimate from the saturation gradient, but hard to get an exact number. As mentioned earlier, this is because of natural variations in the saturation due to heterogeneities in the sandstone, and taking gradients of these variations is difficult. This is why the criteria were developed, to determine the general rules under which the capillary gradient can be discounted. But still, even within these criteria, there is likely to be a systematic variation of the capillary gradient versus position, and that this variation ends up affecting the measured relative permeabilities.

This systematic variation is likely leading to the “Γ” shape in the data for each time interval. This is because ignoring the capillary forces can only result in an under-estimated relative permeability as the capillary forces act to lower the overall gradient, and the assumption is that the gradient does not have these forces. For each time interval, since the highest relative permeability data are at the knee of the “Γ” shape, these are likely to have the smallest capillary forces and be the least biased. This makes sense with our criteria, and the “Γ” shape. The bottom of the leg of the “Γ” shape is when the flux is low – these points are near the top of the column where the inlet capillary gradient is highest (DiCarlo, 2003). Going downward in the column increases the flux (and recorded relative permeability) and reduces the inlet capillary gradient. This is the case for a while, but going further downward, the saturation starts to increase much faster than the flux, producing the top part of the “Γ” shape. Here the saturation is higher than expected due to the increasing capillary gradient toward the outlet of the column (DiCarlo, 2003). This again causes an underestimation of the relative permeability data using this method. The knee in the “Γ” shape is the sweet spot, where the capillary gradient is at a minimum, and thus are the most accurate relative permeabilities.

As shown in Figs. 8 through 11, depending on the flow rate and the time interval, different parts of the “Γ” shape are observed. For instance, in Fig. 8, from each time interval there are 10 points corresponding to saturations and fluxes at 2 cm spatial intervals. These 10 points form a “Γ” shape because as one heads downstream (or down column) both the flux and the saturation increase. Near the top of the 20 cm interval, the flux (which in turn becomes the relative permeability) increases faster than the saturation – this forms the vertical leg of the “Γ” shape. Near the bottom of the interval, the saturation increases faster than the flux – this forms the horizontal top of the “Γ” shape. This shape is most representative for the data around a saturation of 0.5 (this is for time interval 1123 and 1850 min). For earlier times (and higher saturations and fluxes), the vertical shape is prevalent over the top part, and for later times (and lower saturations) the horizontal top is prevalent.

Therefore, early data (high saturation) are more affected by the inlet boundary, while late data (low saturation), the capillary gradients from the outlet play more of a role. But in general, the deviations in the relative permeabilities for one time interval of data are at most a factor of 50% from the general curve. This is true even at the greatest distance away from the knee for the inlet and the outlet. This shows that the capillary forces can be safely ignored as long as one chooses positions that matches the criteria; going further out in position (to the outlet and inlet) and stretching the criteria produces much greater deviations. This also can be seen in

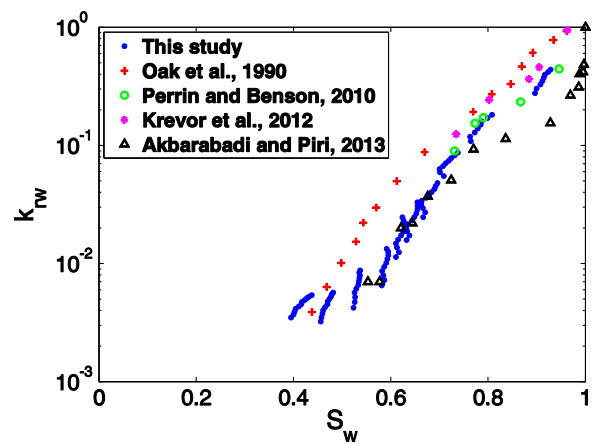


Fig. 14. The water relative permeability curve obtained in this study for Berea core along with those of Berea core samples published in the literature, on log scale.

the difference between Fig. 8 and Fig. 11. In Fig. 11, the capillary gradient is the highest, leading to the largest “Γ” shape and variations. Fig. 12 shows that when all the data are brought together, one main curve is obtained.

6.3. Water relative permeability of Berea sandstone in literature

As another way to validate our method, we compare our data to other experimental water relative permeability data measured on Berea samples. Fig. 14 shows four sets of published water relative permeability data of Berea core samples using steady-state method along with the water relative permeability measured in this study (Oak et al., 1990; Perrin and Benson, 2010; Krevor et al., 2012; Akbarabadi and Piri, 2013). Fig. 14 indicates that the relative permeabilities obtained in this work are in good agreement with those of the literature on Berea core samples over the entire saturation space. In addition, this method results in relative permeabilities over a wide range of saturations while the steady-state method results in only a limited number of points on the relative permeability curve.

7. Conclusions

In this work, we extended a relative permeability method to directly measure relative permeabilities during gravity drainage experiments from unsteady-state in situ saturation profiles in consolidated rocks. We injected gas at the inlet of the core at pressures higher than entry pressure of the rock to allow liquids to drain by gravity to (a) apply a gravity drainage method to consolidated rocks, and (b) extend measurements to larger saturation space. From this work, the following conclusions can be drawn:

- The gravity drainage method allows calculation of relative permeabilities quickly over a large saturation space and provides many points on relative permeability curve.
- The obtained relative permeabilities from this method have high accuracy due to direct measurement of relative permeabilities from unsteady-state in situ saturations. In addition, it is assured that the data are not compromised by capillary entry and end effects.
- Extremely small relative permeabilities (10^{-4} – 10^{-5}) can be obtained from this method.

- It is essential to incorporate the correct gas pressure gradient into the relative permeability calculations by removing the pressure drops at the outlet of the core due to capillary effects.
- No prior knowledge of the P_c curve is needed because capillary pressure is negligible if the mentioned criteria are met.

Acknowledgment

We gratefully acknowledge the gas enhanced oil recovery joint industry project (JIP) at the University of Texas at Austin for their financial support of this work. The relative permeability versus saturation data is available upon request by emailing David A. DiCarlo or Amir Kianinejad at dicarlo@mail.utexas.edu or kianinejad.amir@utexas.edu.

References

- Akbarabadi, Morteza, Piri, Mohammad, 2013. Relative permeability hysteresis and capillary trapping characteristics of supercritical CO₂/brine systems: an experimental study at reservoir conditions. *Adv. Water Resour.* 52, 190–206. <http://dx.doi.org/10.1016/j.advwatres.2012.06.014>.
- Braun, Edward M., Blackwell, Robert J., 1981. A steady-state technique for measuring oil-water relative permeability curves at reservoir conditions. *SPE-10155-MS*. Society of Petroleum Engineers <http://dx.doi.org/10.2118/10155-MS>.
- Brooks, R.H., A.T. Corey. 1964. "Hydraulic properties of porous media." *Hydrology Papers, Colorado State University*, no. March.
- Dehghanpour, H., Aminzadeh, B., Mirzaei, M., DiCarlo, D.A., 2011. Flow coupling during three-phase gravity drainage. *Phys. Rev. E* 83 (6), 065302.
- Dehghanpour, Hassan, DiCarlo, David, 2013. A comparative study of transient and steady-state three-phase oil permeability. *J. Can. Petrol. Technol.* 52 (1), 54–63.
- Dehghanpour, Hassan, DiCarlo, David A., Aminzadeh, Behdad, Galeh-Kalaei, Mohammad Mirzaei, 2010. Two-phase and three-phase saturation routes and relative permeability during fast drainage. *SPE-129962-MS*. Society of Petroleum Engineers.
- Dehghanpour, H., DiCarlo, D.A., 2013. Drainage of capillary-trapped oil by an immiscible gas: impact of transient and steady-state water displacement on three-phase oil permeability. *Trans. Porous Media* 100 (2), 297–319. <http://dx.doi.org/10.1007/s11242-013-0217-z>.
- DiCarlo, D.A., Akshay, Sahni, Blunt, M.J., 2000. Three-phase relative permeability of water-wet oil-wet and mixed-wet sandpacks. *SPE J.* 5 (01), 82–91.
- DiCarlo, David A., 2003. Drainage in finite-sized unsaturated zones. *Adv. Water Resour.* 26 (12), 1257–1266. <http://dx.doi.org/10.1016/j.advwatres.2003.09.001>.
- DiCarlo, David A., Sahni, Akshay, Blunt, Martin J., 2000. The effect of wettability on three-phase relative permeability. *Trans. Porous Media* 39 (3), 347–366.
- Fassilhi, Mohammad Reza, Potter, Gary Frank, 2009. Analysis of transient data during relative permeability measurements using steady-state technique. *SPE-123676-MS*. Society of Petroleum Engineers.
- Geffen, T.M., Owens, W.W., Parrish, D.R., Morse, R.A., 1951. Experimental investigation of factors affecting laboratory relative permeability measurements. *SPE-951099-G* <http://dx.doi.org/10.2118/951099-G>.
- Grader, A.S., O'Meara Jr., D.J., 1988. Dynamic displacement measurements of three-phase relative permeabilities using three immiscible liquids. *SPE-18293-MS*. Society of Petroleum Engineers.
- Hagoort, J., 1980. Oil recovery by gravity drainage. *SPE-7424-PA* <http://dx.doi.org/10.2118/7424-PA>.
- Honarpour, M., Mahmood, S.M., 1988. Relative-permeability measurements: an overview. *J. Petrol. Technol.* 40 (08), 963–966.
- Johnson, E.F., Bossler, D.P., Naumann, V.O., 1959. Calculation of relative permeability from displacement experiments. *Petrol. Trans. AIME*, SPE-1023-G 216 (January), 370–372.
- Jones, S.C., Roszelle, W.O., 1978. Graphical techniques for determining relative permeability from displacement experiments. *SPE-6045-PA* <http://dx.doi.org/10.2118/6045-PA>.
- Kerig, P.D., Watson, A.T., 1987. A New Algorithm for estimating relative permeabilities from displacement experiments. *SPE-14476-PA* <http://dx.doi.org/10.2118/14476-PA>.
- Kianinejad, Amir, Aminzadeh, Behdad, Chen, Xiongyu, DiCarlo, David A., 2014. Three-phase relative permeabilities as a function of flow history. *SPE-169083-MS*. Society of Petroleum Engineers <http://dx.doi.org/10.2118/169083-MS>.
- Kianinejad, Amir, Chen, Xiongyu, DiCarlo, David A., 2015. The effect of saturation path on three-phase relative permeability. *Water Resour. Res.* 51 (11), 9141–9164. <http://dx.doi.org/10.1002/2015WR017185>.
- Krevor, Samuel C.M., Pini, Ronny, Zuo, Lin, Benson, Sally M., 2012. Relative permeability and trapping of CO₂ and water in sandstone rocks at reservoir conditions. *Water Resour. Res.* 48 (2), W02532. <http://dx.doi.org/10.1029/2011WR010859>.
- Maini, B.B., Batycky, J.P., 1985. Effect of temperature on heavy-oil/water relative permeabilities in horizontally and vertically drilled core plugs. *SPE-12115-PA* <http://dx.doi.org/10.2118/12115-PA>.
- Maini, B.B., Okazawa, T., 1987. Effects of temperature on heavy oil-water relative permeability of sand. *PETSOC-87-03-03* <http://dx.doi.org/10.2118/87-03-03>.
- Mohanty, K.K., Miller, A.E., 1991. Factors influencing unsteady relative permeability of a mixed-wet reservoir rock. *SPE Form. Eval.* 6 (03), 349–358.
- Mohsenzadeh, Adel, Nabipour, Moein, Asadizadeh, Sajad, Nekouie, Mohsen, Ameri, Abolhasan, Ayatollahi, Shahab, 2011. Experimental investigation of different steam injection scenarios during SAGD process. *Special Topics Rev. Porous Media: An Int. J.* 2 (4), 283–291. <http://dx.doi.org/10.1615/SpecialTopicsRevPorousMedia.v2.i4.30>.
- Naylor, P., Sargent, N.C., Crosbie, A.J., Tilsed, A.P., Goodyear, S.G., 1996. Gravity drainage during gas injection. *Petrol. Geosci.* 2 (1), 69–74.
- Oak, M.J., 1990. Three-phase relative permeability of water-wet Berea. *SPE-20183-MS*. Society of Petroleum Engineers.
- Oak, M.J., Baker, L.E., Thomas, D.C., 1990. Three-phase relative permeability of Berea sandstone. *SPE-17370-PA* <http://dx.doi.org/10.2118/17370-PA>.
- Osoba, J.S., Richardson, J.G., Kerver, J.K., Hafford, J.A., Blair, P.M., 1951. Laboratory measurements of relative permeability. *SPE-951047-G* <http://dx.doi.org/10.2118/951047-G>.
- Perrin, Jean-Christophe, Benson, Sally, 2010. An experimental study on the influence of sub-core scale heterogeneities on CO₂ distribution in reservoir rocks. *Trans. Porous Media* 82 (1), 93–109. <http://dx.doi.org/10.1007/s11242-009-9426-x>.
- Pini, Ronny, Benson, Sally M., 2013. Simultaneous determination of capillary pressure and relative permeability curves from core-flooding experiments with various fluid pairs. *Water Resour. Res.* 49 (6), 3516–3530. <http://dx.doi.org/10.1002/wrcr.20274>.
- Rapoport, L.A., Leas, W.J., 1953. Properties of linear waterfloods. *Trans. AIME* 198 (1953), 139–148.
- Rezaveisi, M., Rostami, Behzad, Kharrat, Riyaz, Ayatollahi, Shahab, Ghotbi, C., 2010. Experimental investigation of tertiary oil gravity drainage in fractured porous media. *Special Topics Rev. Porous Media: An Int. J.* 1 (2), 179–191. <http://dx.doi.org/10.1615/SpecialTopicsRevPorousMedia.v1.i2.70>.
- Richards, L.A., 1931. Capillary conduction of liquids through porous mediums. *J. Appl. Phys.* 1 (5), 318–333.
- Richardson, J.G., Kerver, J.K., Hafford, J.A., Osoba, J.S., 1952. Laboratory determination of relative permeability. *SPE-952187-G* <http://dx.doi.org/10.2118/952187-G>.
- Sahni, Akshay, Burger, Jon, Blunt, Martin, 1998. Measurement of three phase relative permeability during gravity drainage using CT. *SPE-39655-MS*. Society of Petroleum Engineers.
- Saraf, Deoki N., Batycky, James P., Jackson, Clive H., Fisher, Douglas B., 1982. An experimental investigation of three-phase flow of water-oil-gas mixtures through water-wet sandstones. *SPE-10761-MS*. Society of Petroleum Engineers.
- Sarem, A.M., 1966. Three-phase relative permeability measurements by unsteady-state method. *Soc. Petrol. Eng. J.* 6 (03), 199–205.
- Siddiqui, S., Hicks, P.J., Grader, A.S., 1996. Verification of Buckley–Leverett three-phase theory using computerized tomography. *J. Petrol. Sci. Eng.* 15 (1), 1–21. [http://dx.doi.org/10.1016/0920-4105\(95\)00056-9](http://dx.doi.org/10.1016/0920-4105(95)00056-9).
- Sigmund, P.M., McCaffery, F.G., 1979. An improved unsteady-state procedure for determining the relative-permeability characteristics of heterogeneous porous media (includes associated papers 8028 and 8777). *SPE-6720-PA* <http://dx.doi.org/10.2118/6720-PA>.
- Virnovskii, G.A., 1984. Determination of relative permeabilities in a three-phase flow in a porous medium. *Fluid Dyn.* 19 (5), 835–837. <http://dx.doi.org/10.1007/BF01093558>.
- Vizika, Olga, Lombard, J.M., 1996. Wettability and spreading: two key parameters in oil recovery with three-phase gravity drainage. *SPE Reser. Eng.* 11 (1), 54–60.
- Welge, H.J., 1950. Displacement of oil from porous media by water and gas. *Trans. AIME* 198, 314–316.
- Zhou, Degen, Blunt, Martin, 1997. Effect of spreading coefficient on the distribution of light non-aqueous phase liquid in the subsurface. *J. Contaminant Hydrol.* 25 (1), 1–19. [http://dx.doi.org/10.1016/S0169-7722\(96\)00025-3](http://dx.doi.org/10.1016/S0169-7722(96)00025-3).